Molecular mechanism of point mutation-induced Monopolar spindle 1 (Mps1/TTK) inhibitor resistance revealed by a comprehensive molecular modeling study

Yan Han[1], Yungang Wu[1], Yi Xu[2], Wentao Guo[3], Na Zhang[1] and Xiaoyi Wang[1]

[1] Department of TCM Orthopedics & Traumatology, the First Affiliated Hospital of Wenzhou Medical University, Wenzhou, Zhejiang, China
[2] Department of Pharmacy, the First Affiliated Hospital of Wenzhou Medical University, Wenzhou, Zhejiang, China
[3] School of Pharmacy, Wenzhou Medical University, Wenzhou, Zhejiang, China

ABSTRACT

Background. Monopolar spindle 1 (Mps1/TTK) is an apical dual-specificity protein kinase in the spindle assembly checkpoint (SAC) that guarantees accurate segregation of chromosomes during mitosis. High levels of Mps1 are found in various types of human malignancies, such as glioblastoma, osteosarcoma, hepatocellular carcinoma, and breast cancer. Several potent inhibitors of Mps1 exist, and exhibit promising activity in many cell cultures and xenograft models. However, resistance due to point mutations in the kinase domain of Mps1 limits the therapeutic effects of these inhibitors. Understanding the detailed resistance mechanism induced by Mps1 point mutations is therefore vital for the development of novel inhibitors against malignancies.

Methods. In this study, conventional molecular dynamics (MD) simulation and Gaussian accelerated MD (GaMD) simulation were performed to elucidate the resistance mechanisms of Cpd-5, a potent Mps1 inhibitor, induced by the four representative mutations I531M, I598F, C604Y, S611R.

Results. Our results from conventional MD simulation combined with structural analysis and free energy calculation indicated that the four mutations weaken the binding affinity of Cpd-5 and the major variations in structural were the conformational changes of the P-loop, A-loop and αC-helix. Energetic differences of per-residue between the WT system and the mutant systems indicated the mutations may allosterically regulate the conformational ensemble and the major variations were residues of Ile-663 and Gln-683, which located in the key loops of catalytic loop and A-loop, respectively. The large conformational and energetic differences were further supported by the GaMD simulations. Overall, these obtained molecular mechanisms will aid rational design of novel Mps1 inhibitors to combat inhibitor resistance.

Subjects Computational Biology, Oncology
Keywords Mutation, Monopolar spindle 1, Resistance mechanism, Molecular dynamics simulation

INTRODUCTION

Mammalian cell division is accurately regulated by activation and inactivation of related proteins that manage progression through the phases of the cell cycle (*Bertoli, Skotheim & De Bruin, 2013*). To ensure segregation of duplicated chromosome during mitosis and meiosis, cell-cycle checkpoints have evolved that play essential roles in genome maintenance under varieties of stress conditions (*Barnum & O'Connell, 2014*). The spindle assembly checkpoint (SAC), one of cell-cycle checkpoints and a signaling cascade, prevents chromosome missegregation by delaying mitotic progression until all chromosomes are correctly attached to spindle microtubules (*Hiruma et al., 2015*). Inactivation of SAC leads to premature anaphase onset, and, therefore, chromosomal instability and aneuploidy, which is responsible for cell death or tumorigenesis (*De Carcer, Perez de Castro & Malumbres, 2007*; *Marques et al., 2015*; *Salmela & Kallio, 2013*).

The mono-polar spindle 1 (Mps1, also called TTK), one of the main components of SAC, is generally regarded as a master conductor of SAC signaling, which recruit in early mitosis to unattached kinetochores (*Pachis & Kops, 2018*). Mps1 has been proposed to be dysregulated in various cancer cells (*Xie et al., 2017*). For instance, mRNA expression of Mps1 is elevated in numerous of cancers relative to normal tissue. These include glioblastoma, osteosarcoma, hepatocellular carcinoma, breast cancer, and other cancers. Reduction in Mps1 levels or activity in these tumors can lead to loss of cell viability; therefore, inhibition of Mps1 has been regard as an attractive strategy to target cancers, especially those with chromosomal instability (*Daniel et al., 2011*; *Xie et al., 2017*). Many structurally diverse Mps1 inhibitors have been reported and have undergone preclinical assessments in recent years, such as NMS-P715, Cpd-5, CCT251455, MPS1-IN-3, reversine, MPI-0479605, AZ3146 (*Colombo et al., 2010*; *Hewitt et al., 2010*; *Hiruma et al., 2017*; *Naud et al., 2013*; *Tannous et al., 2013*; *Tardif et al., 2011*). Unfortunately, in cancer cells, the resistance to Mps1 inhibitors eventually occurs and this resistance is mostly due to mutations in the conserved ATP binding pocket of the Mps1 kinase domain, which leads to a remarkably attenuation of the therapeutic efficiency of the Mps1 inhibitors (*Hiruma et al., 2017*; *Koch et al., 2016*).

The kinase domain of Mps1 adopts a bi-lobal structure, a smaller N-terminal domain, and a larger C-terminal domain connected by kinase hinge, which together form the catalytic site to ensure the transfer of a phosphate from adenosine triphosphate (i.e., ATP) to a substrate hydroxyl (Fig. 1A). The N-terminal domain contains six stranded antiparallel β-sheets, an important regulatory αC-helix, and a phosphate binding loop (i.e., P-loop). The C-terminal domain consists of seven α-helices, two β-sheets, a catalytic loop, and an essential activation loop (i.e., A-loop, residues 676–685) (*Chu et al., 2008*; *Wang et al., 2009*). Recently, *Koch et al. (2016)* reported four point mutations (I531M, I598F, C604Y, S611R) in the kinase domain of Mps1 that gave rise to the Cpd-5 resistance, but retained wild type (WT) catalytic activity. Cpd-5 (N-(2,6-diethylphenyl)-8-((2-methoxy-4-(4-methylpiperazin-1-yl)phenyl)amino)-1-methyl-4,5-dihydro-1H-pyrazolo[4,3h] quinazoline-3 carboxamide), a derivative of NMS-P715, has been reported to display higher potency toward Mps1 than NMS-P715, reversine, MPI-0479605 (*Koch et al., 2016*).
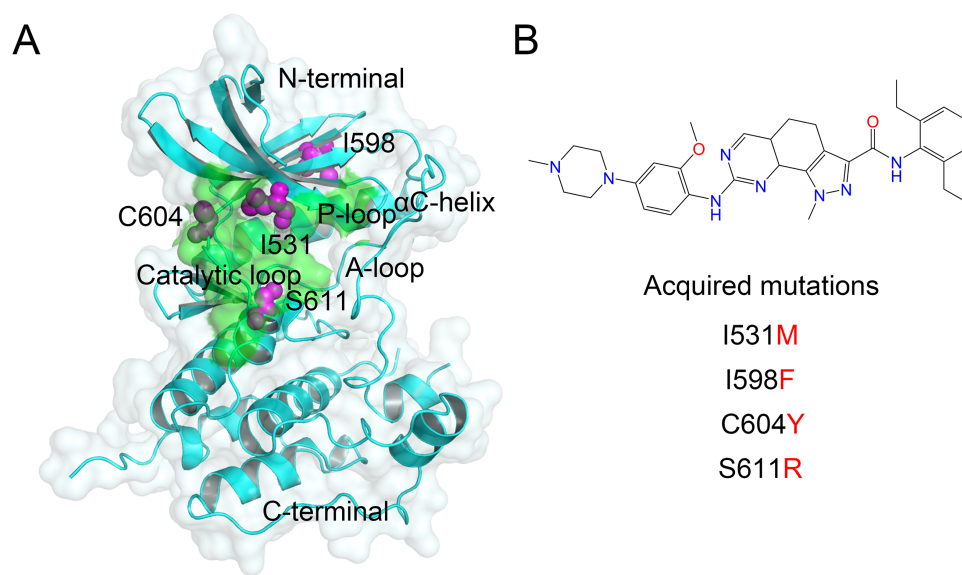
Figure 1 **Overview of the kinase domain of Mps1 and point mutations.** (A) Overview the structure of the Mps1 kinase domain. The point mutations of I531M, I598F, C604Y, S611R are colored magenta balls. (B) Two-dimensional structure of Cpd-5.

Full-size ◰ DOI: 10.7717/peerj.6299/fig-1

Recently, *Chen et al. (2018)* reported resistance mechanisms of inhibitors to Mps1 C604Y Mutation, however, it is not clear from the structures why other mutations (I531M, I598F, S611R) would cause resistance. Molecular dynamics (MD) simulations may be helpful to explain these resistance mutations by monitoring the dynamics of the protein and its interactions with bound inhibitors.

In this study, the WT Mps1 (Mps1^{WT}) and four mutants associated with Cpd-5 resistance, including I531M (Mps1^{I531M}), I598F (Mps1^{I598F}), C604Y (Mps1^{C604Y}), S611R (Mps1^{S611R}), were chosen to create an overall view of the structural dynamics. Herein, conventional molecular dynamics (MD) simulations combined with structural analysis and Molecular Mechanics/Generalized Born Surface Area (MM/GBSA) free energy calculations were employed to elucidate the impact of point mutations on the conformational and energetic difference between WT and mutant systems. In addition, Gaussian accelerated molecular dynamics (GaMD) simulations in conjunction with structural analysis, principal component analysis (PCA) and 2D free energy calculations were performed to sample more conformational space due to conventional MD simulation remains limited conformational ensembles. Overall, the comprehensive molecular modeling study performed in this study can be effective to study the resistance mechanism. More importantly, the insights from this study may have an essential application in designing novel Mps1 inhibitors to combat inhibitor resistance.

MATERIALS & METHODS

Construct the initial structures of Mps1^{WT}, Mps1^{I531M}, Mps1^{I598F}, Mps1^{S611R}

The three-dimensional structure of the Mps1^{C604Y}/Cpd-5 complex was retrieved from Protein Data Bank (PDB) database (PDB entry: 5MRB) (*Hiruma et al., 2017*). Mps1^{WT}, Mps1^{I531M}, Mps1^{I598F}, Mps1^{S611R} were constructed by using the EasyModeller program by substituting specific residues (*Fiser & Sali, 2003*; *Kuntal, Aparoy & Reddanna, 2010*). Then, the modeled structures were refined by Chimera software, including modelling the A-loop, adding missing side-chains and missing hydrogen atoms (*Pettersen et al., 2004*).

Conventional molecular dynamics (MD) simulations

The crystal structure of Mps1^{C604Y}/Cpd-5, and the modeled structures of Mps1^{WT}/Cpd-5, Mps1^{I531M}/Cpd-5, Mps1^{I598F}/Cpd-5, Mps1^{S611R}/Cpd-5 were used as the initial structures for the conventional MD simulations. Prior to conventional MD simulations, the force field parameters for the proteins and ligands were generated using LEaP module in Amber 16 software with AMBER ff14SB force field and general Amber force field 2 (GAFF2). Thereafter, each system was immersed in a water box by the TIP3P water model with at least a 12 Å distance around the protein-ligand complex. Finally, an appropriate number of counter ions were added to keep the electroneutrality.

Before each productive MD simulation, a sophisticated protocol was applied, including minimization, heating and equilibration. The first step of energy minimization was to employed a harmonic restraint of 5 kcal mol^{-1} Å^{-2} to the solute and side chains of protein. The second step was to allow all atoms to move freely without any restraint. In each step, minimization was performed using the steepest descent algorithm for the first 5,000 steps and the conjugated gradient algorithm for the succeeding 5,000 steps. Afterwards, each system was heated to 310 K in the NVT ensemble using a Langevin thermostat with harmonic restraints of 4 kcal mol^{-1} Å^{-2}. Then, 1ns unconstrained NPT dynamics at 310 K and 1 bar was applied to equilibrate each system. Lastly, 240 ns productive conventional MD simulations were carried out under the NPT condition. During the simulations, Periodic boundary condition, Langevin temperature scaling, Particle Mesh Ewald (PME) algorithm with cutoff 8.0 Å and SHAKE algorithm was applied (*Essmann et al., 1995*; *Izaguirre et al., 2001*; *Kräutler, Van Gunsteren & Hünenberger, 2001*). A time step of 2 fs was performed and coordinates were recorded every 2 ps for further analysis.

End-point free energy calculations

The binding free energy (ΔG_{calc}) of Cpd-5 binding to Mps1^{WT}, Mps1^{I531M}, Mps1^{I598F}, Mps1^{C604Y}, Mps1^{S611R} was calculated by using the end-point molecular mechanics generalized Born surface area (MM/GBSA). The MM/GBSA approach has been extensively used in understanding the mechanisms of mutation-induced drug resistance (*He et al., 2018*; *Liu et al., 2017*; *Pan et al., 2013*). The ΔG_{calc} was computed by using the following equations:

$$\Delta G_{calc} = \Delta E_{MM} + \Delta G_{sol} - T\Delta S \tag{1}$$

$$\Delta E_{MM} = \Delta E_{int} + \Delta E_{vdW} + \Delta E_{elec} \tag{2}$$

$$\Delta G_{sol} = \Delta G_{GB} + \Delta G_{SA} \tag{3}$$

$$\Delta G_{SA} = \gamma \Delta A + b \tag{4}$$

where ΔE_{MM}, ΔG_{sol}, and $-T\Delta S$ represent the molecular mechanics interaction energy, solvation energy, and entropy term (Eq. 1). In Eq. 2, the ΔE_{MM} consists of the change of internal energy (ΔE_{int}), van der Waals energy (ΔE_{vdW}), and electrostatic energy (ΔE_{elec}). In Eq. 3, the ΔG_{sol} contains the polar part (ΔG_{GB}) and the nonpolar part of the desolvation energy (ΔG_{SA}). In this study, ΔE_{int} was canceled by using a single trajectory strategy in order to reduce the noise (*Sun et al., 2013*). The ΔG_{GB} was calculated using a GB^{OBC1} model (igb = 2) (*Onufriev, Bashford & David, 2000*). The ΔG_{SA} was calculated by Eq. 4. Where ΔA is the change of the solvent accessible surface area (SASA), and the fitting coefficients γ and b were set to 0.0072 kcal mol^{-1}Å^{-2} and 0, respectively. Simulation trajectories from 200 to 240 ns with 200 snapshots were employed to binding free energy calculations and free energy decompositions.

Gaussian accelerated molecular dynamics (GaMD) simulation

The equilibrated structures extracted from conventional MD simulation trajectories were chosen as the initial structure for the GaMD simulations. During GaMD simulations, a non-negative harmonic boost potential is added to smooth the studied system potential energy surface in order to decrease the energy barriers and accelerate the conformational sampling (*Miao & McCammon, 2016a*; *Miao & McCammon, 2016b*). When the system potential $V(\vec{r})$ is lower than a threshold energy (E), a harmonic boost potential $V^*(\vec{r})$ is added as Eq. (5). k is the harmonic force constant. When the system potential is above the E, the boost potential is set to zero as Eq. (6).

$$V^*(\vec{r}) = V(\vec{r}) + \frac{1}{2}k(E - V(\vec{r}))^2 \quad V(\vec{r}) < E \tag{5}$$

$$V^*(\vec{r}) = V(\vec{r}) \quad V(\vec{r}) \geq E \tag{6}$$

GaMD simulation provides the total potential boost, dihedral potential boost, and dual potential boost in order to accelerate the MD simulations. Herein, dual potential boost was applied to the GaMD simulations. The dual potential boost parameters were computed from an initial ~4 ns NVT conventional MD simulation without any potential boost. Afterwards, 1 ns GaMD simulation were performed, in which the potential boost was updated every 100 ps to reach equilibrium values. Eventually, 400 ns GaMD simulation for each system was submitted in the NVT ensemble. During the simulations, the temperature was regulated using a Langein thermostat. PME algorithm and the non-bonded with cutoff 10.0 Å to consider the long-range electrostatic interactions and non-bonding interactions (*Essmann et al., 1995*). Atomic coordinate trajectory was recorded every 2 ps.

Principal component analysis (PCA) and free energy calculations for the GaMD simulations

PCA calculations contain diagonalization of the covariance matrix of positional deviations among a structural ensemble. The structures from MD simulation trajectories were aligned

to remove the translational and rotational motions. PCA was performed for the trajectories of 400 ns GaMD simulations by using the Bio3D package of R (*Skjaerven et al., 2014*). Thereafter, the potential boost combined with the principal component 1 (PC1) and principal component 2 (PC2) calculated from PCA were applied to recover the free energy map by cumulant expansion to the 2nd order method (*Miao et al., 2014*; *Roe & Cheatham 3rd, 2013*).

RESULTS AND DISCUSSION

The overall structural properties

The structural dynamics of Cpd-5 bound with WT Mps1 or mutant Mps1 were analyzed by performing 240 ns conventional MD simulations. To qualitatively investigate the stability and overall convergence of the simulated systems, the root mean square deviation (RMSD) of protein backbone atoms, and the heavy atoms of the Cpd-5 were calculated and plotted against time in Figs. 2 and 3. As plotted in Fig. 2, all the RMSD values of backbone atoms of Mps1 have a small fluctuation after 50–170 ns, indicating all the systems achieve equilibrium at ∼50–170 ns. The RMSD of the heavy atoms of the Cpd-5 in each system maintained relative stable (RMSD < 2 Å) during the 240 ns simulation (Fig. 3). As expected, the average RMSD values of both the Mps1 protein and the Cpd-5 follow the order of WT systems <mutant systems (Figs. 2 and 3). These findings are directly consistent with the experimental data that Cpd-5 is more stable in WT Mps1 than in the mutants. Thereafter, the trajectories of the last 60 ns simulations were extracted for the following structural and energetic analysis.

Then, the root-mean-square fluctuations (RMSFs) of the protein backbone, which represents the flexibility and mobility of protein backbone, were calculated and averaged for all the simulated systems to evaluate the local structure transformations in more detail. As shown in Fig. 4, all the simulated systems share similar RMSF distributions and similar trends of dynamics features. However, we noticed the P-loop region of Mps1^{I531M}, Mps1^{I598F}, Mps1^{C604Y}, the αC-helix region of Mps1^{I598F}, the A-loop region of all the four mutant systems, which exhibited amplified fluctuations when these regions were compared to WT system. The alignment of the last snapshot between WT (yellow) system and mutant (cyan) systems showed a highly similar pattern with minor adjustments in the regions of P-loop, αC-helix, A-loop (Fig. 5). For instance, compared with Mps1^{WT}, the P-loop region of Mps1^{I531M}, Mps1^{I598F}, Mps1^{C604Y} and the αC-helix region of Mps1^{I598F} change into upward-moving conformation compared with Mps1^{WT} (Figs. 5B–5D). The A-loop region of mutant systems showed an outward-moving conformation (Figs. 5A–5D). This finding was also consistent with the previous study that when Mps1 binds with Cpd-5, the A-loop region of Mps1^{C604Y} changes into an outward-moving conformation, but not the Mps1^{WT} (*Chen et al., 2018*). Compared with the previous results, we also found that the P-loop had a slight conformational change (*Chen et al., 2018*), particularly in Mps1^{I598F} and Mps1^{C604Y} systems. Overall, these results indicated that mutation-induced conformational change might be the main driving force for the redistributed energies. Hence, the MM/GBSA approach was employed to determine the key molecular determinants.
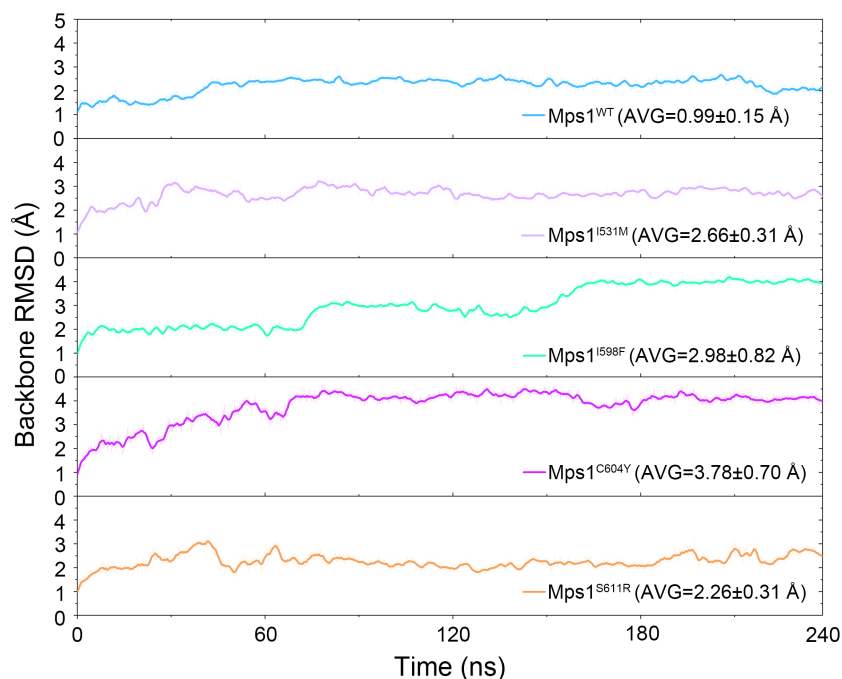
Figure 2 **Time evolution of the RMSD values of backbone atoms of the Mps1 protein in the five studied systems from conventional MD simulations.** The values reflect the equilibration of each protein relative to the initial structures.

Binding free energy and decomposition analysis

As an important complement to the binding mode and structural analysis discussed above, the binding free energies of the Cpd-5 to the WT system and the mutant systems calculated from the MM-GBSA approach were summarized in Table 1. According to Table 1, the predicted binding free energies (ΔG_{calc}) of Cpd-5 to Mps1^{WT}, Mps1^{I531M}, Mps1^{I598F}, Mps1^{C604Y}, Mps1^{S611R} were -59.73 ± 4.72, -51.89 ± 4.14, -52.00 ± 4.61, -49.77 ± 3.67, and -54.66 ± 3.74 kcal/mol, respectively. It can be observed that the ΔG_{calc} follow the order of WT systems <mutant systems, that is to say, the ΔG_{calc} show a high correlation with the reported experimental data of IC$_{50}$. Then, individual components of binding free energy were analyzed, which could provide useful information to understand the inhibitor resistance mechanism followed by individual contribution decompositions to the binding free energies. As shown in Table 1, the van der Waals contributions of Cpd-5 to Mps1^{WT}, Mps1^{I531M}, Mps1^{I598F}, Mps1^{C604Y}, Mps1^{S611R} were -73.57 ± 4.62, -62.15 ± 3.78, -63.28 ± 5.09, -61.16 ± 3.89, -66.43 ± 4.28 kcal/mol, respectively, which determine the difference of the binding free energies between WT and mutant systems.

To further probe the interaction between Cpd-5 and Mps1, per-residue decomposition analysis was conducted to obtain a more detailed description of each residue contribution to the binding free energy by MM/GBSA decomposition approach. Energetic differences of per-residue between the WT system and the mutant systems ($\Delta\Delta G = \Delta G_{WT} - \Delta G_{mutant}$) were plotted to highlight the key residues, which induced redistribution of binding free
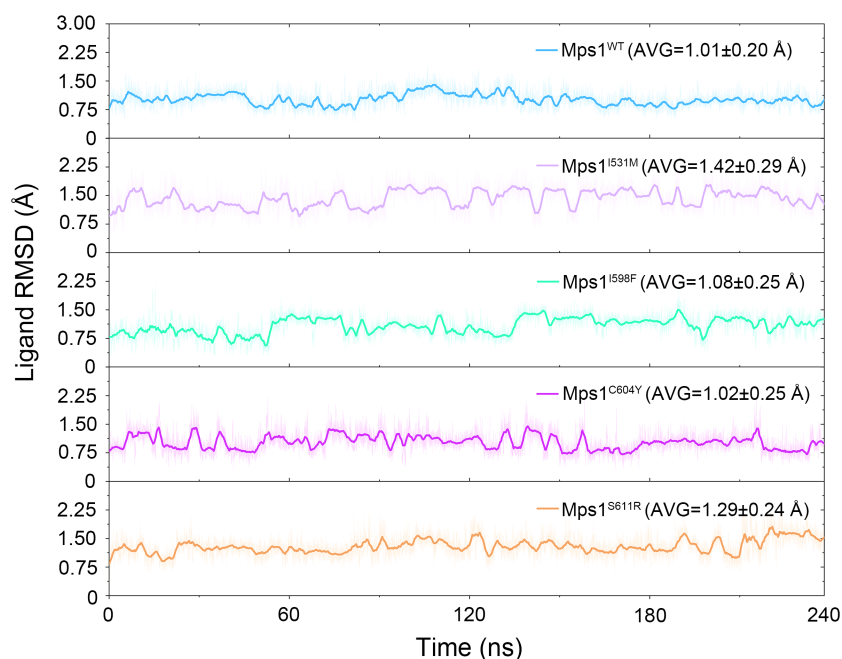
Figure 3 **Time evolution of the RMSD values of cpd-5 in the five studied systems from conventional MD simulations.** The values reflect the equilibration of Cpd-5 in different protein relative to the initial structures.
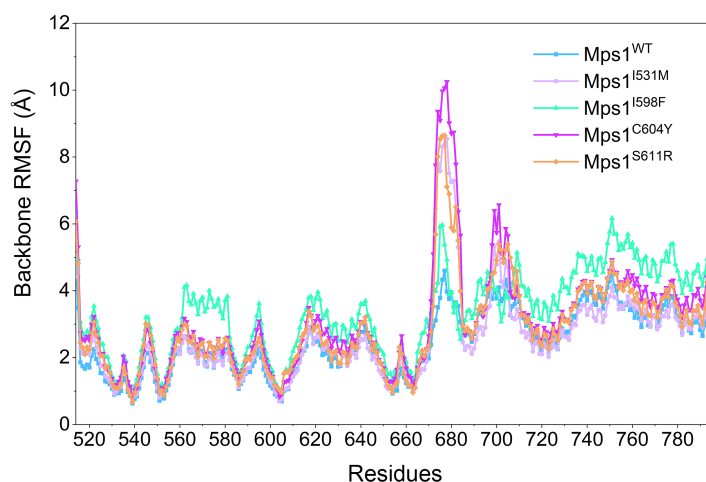
Full-size ⬚ DOI: 10.7717/peerj.6299/fig-3

Figure 4 **RMSFs of backbone atoms versus residue number in the five studied systems from conventional MD simulations.** RMSF provides a picture of overall movement of a residue within a reference frame. A higher RMSF value represents a larger conformational change in spec.

Full-size ⬚ DOI: 10.7717/peerj.6299/fig-4

energy. As shown in Fig. 6, the negative values indicated that the residues of the WT Mps1 protein form stronger interactions with Cpd-5 than the mutant Mps1 protein, while the positive values suggested that the residues of the mutant Mps1 protein form stronger interactions with Cpd-5 than the WT Mps1 protein. As plotted in Fig. 6A, the key residues
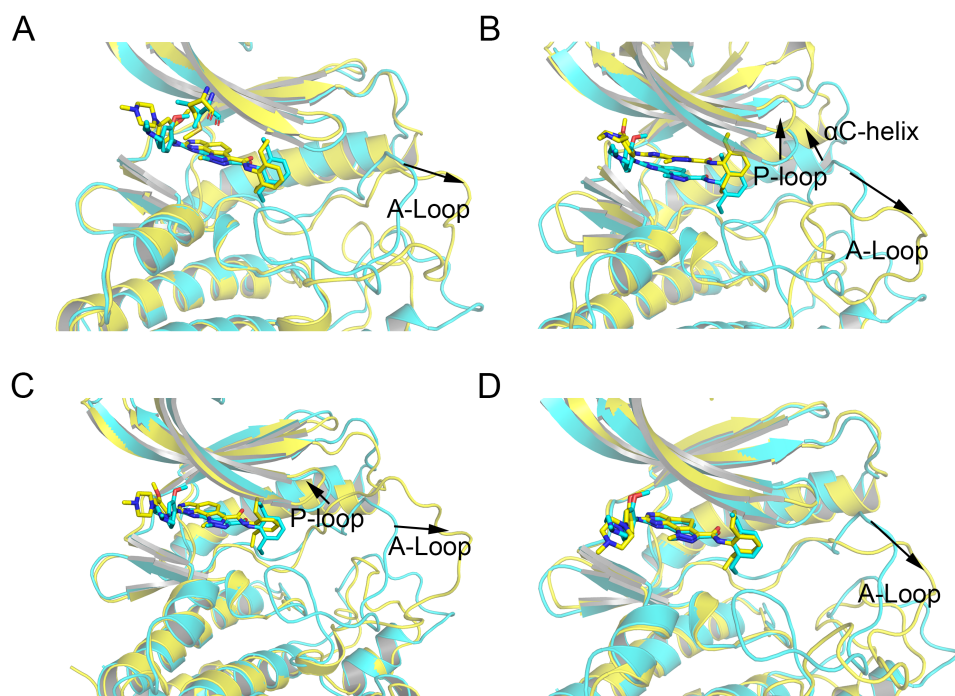
Figure 5 **Alignment of the last snapshot between Mps1^{WT}/cpd-5 and the mutant systems from conventional MD simulations.** (A) Mps1^{WT}/cpd-5 (cyan) and Mps1^{I531M}/Cpd-5 (yellow). (B) Mps1^{WT}/cpd-5 (cyan) and Mps1^{I598F}/Cpd-5 (yellow). (C) Mps1^{WT}/cpd-5 (cyan) and Mps1^{C604Y}/Cpd-5 (yellow). (D) Mps1^{WT}/cpd-5 (cyan) and Mps1^{S611R}/Cpd-5 (yellow).

Full-size 🖼 DOI: 10.7717/peerj.6299/fig-5

Table 1 **Binding free energies of Cpd-5 in WT and mutant systems (kcal/mol).**

Name	ΔE_{vdW}	ΔE_{elec}	ΔG_{GB}	ΔG_{SA}	ΔG_{calc}	IC$_{50}$ (nM)
Mps1^{WT}	-73.57 ± 4.62	-26.98 ± 7.14	49.74 ± 5.95	-8.92 ± 0.48	-59.73 ± 4.72	33.2
Mps1^{I531M}	-62.15 ± 3.78	-27.71 ± 7.11	47.89 ± 5.56	-7.91 ± 0.41	-51.89 ± 4.14	119.0
Mps1^{I598F}	-63.28 ± 5.09	-28.04 ± 7.15	47.37 ± 5.66	-7.72 ± 0.55	-52.00 ± 4.61	72
Mps1^{C604Y}	-61.16 ± 3.89	-30.23 ± 5.44	49.61 ± 4.63	-7.98 ± 0.36	-49.77 ± 3.67	374.8
Mps1^{S611R}	-66.43 ± 4.28	-27.79 ± 6.75	47.75 ± 4.51	-8.18 ± 0.42	-54.66 ± 3.74	129.9

Notes.

ΔE_{vdW}, Van der Waals energy; ΔE_{ele}, electrostatic energy; ΔG_{GB}, electrostatic contribution to solvation; ΔG_{SA}, non-polar contribution to solvation; ΔG_{calc}, binding free energy; IC$_{50}$, half maximal inhibitory concentration.

of Ile-663 and Gln-683 have significant stronger interactions to Cpd-5 in the WT system than in all the mutant systems. Notably, the residues of Ile-663 and Gln-683 are located in the two flexible key loops of catalytic loop and A-loop, respectively, which are important in rotating the Asp-Phe-Gly (DFG) motif into proper orientation for catalysis and substrate binding (Figs. 6B and 6C). These observations may be helpful to aid rational design of novel Mps1 inhibitors to overcome inhibitor resistance. For instance, moderately increasing the hydrophobicity of the compound to interact with Ile-663 to stabilize the catalytic loop and forming hydrogen bonds with Gln-683 to stabilize the A-loop.
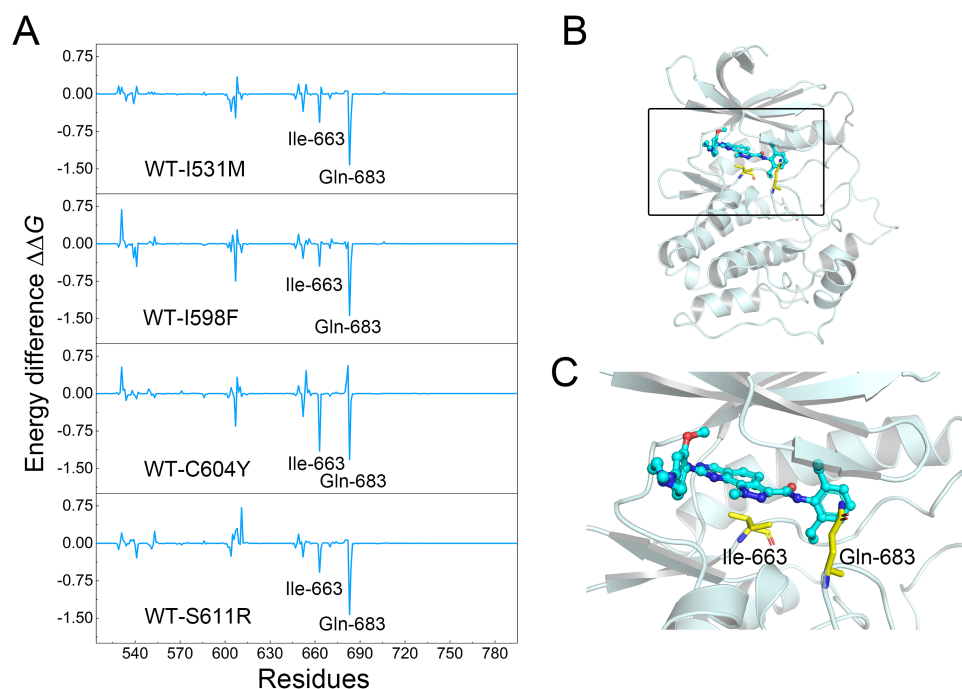
Figure 6 Differences of each residue contribution between the WT system and the mutant systems.
(A) The energetic differences between the WT system and the mutant systems of each residue contribution to Cpd-5 binding; (B) schematic view of the key residues; (C) detailed view of the key residues; (C) detailed view of the key residues.

GaMD simulations

All-atom conventional MD simulations are still limited to the conformational ensembles because of the possible energy barriers between various intermediate states. Therefore, an enhanced sampling method, which can take samples at various intermediate states is required. The traditional enhanced sampling often requires predefined parameters, such as root-mean-square distance atom distances, torsional dihedral, which usually needs expert knowledge of the studied systems. However, the enhanced sampling technique of GaMD simulation avoids such a requirement. In this study, we applied the GaMD simulation technique to further explore more conformational states. Following the initial 240 ns conventional MD simulation, the last snapshot of each system was used as the initial structure to GaMD simulation.

The RMSDs of the protein backbone and the heavy atoms of Cpd-5 with respect to the starting conformations were calculated after alignment of all the conformations from GaMD simulation by removing the rotational and translational motions (Figs. 7 and 8). As shown in Fig. 7, the RMSD of protein backbones of all the systems achieved equilibrium after 30–200 ns GaMD simulations. Figure 8 showed the RMSDs of the heavy atoms of Cpd-5 in each system maintained dynamic constant during the 400 ns of GaMD simulation, indicating the stability of the Cpd-5 in the studied systems.
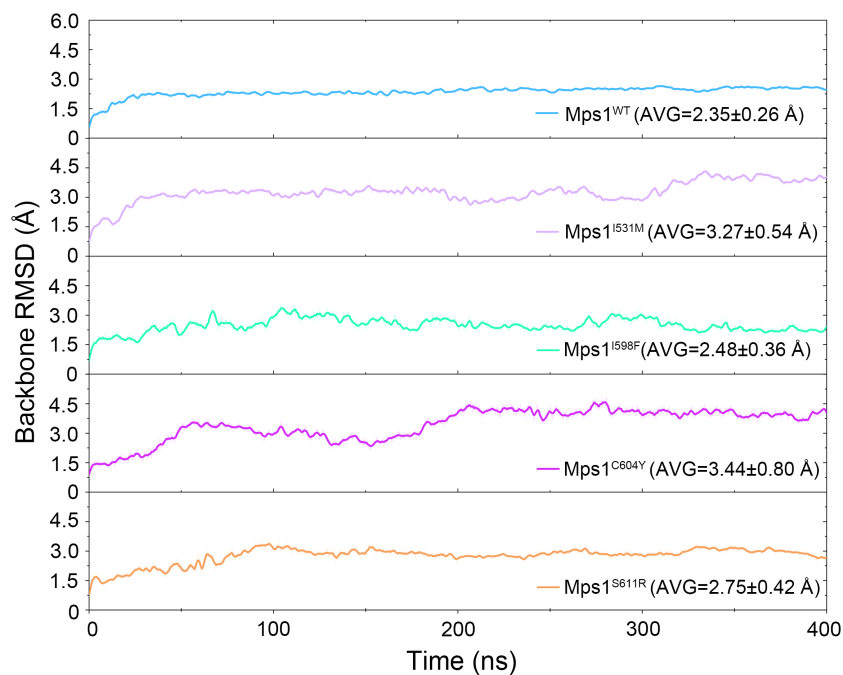
Figure 7 **Time evolution of the RMSD values of backbone atoms of the Mps1 protein in the five studied systems from GaMD simulations.** The values reflect the equilibration of each protein relative to the initial structures.
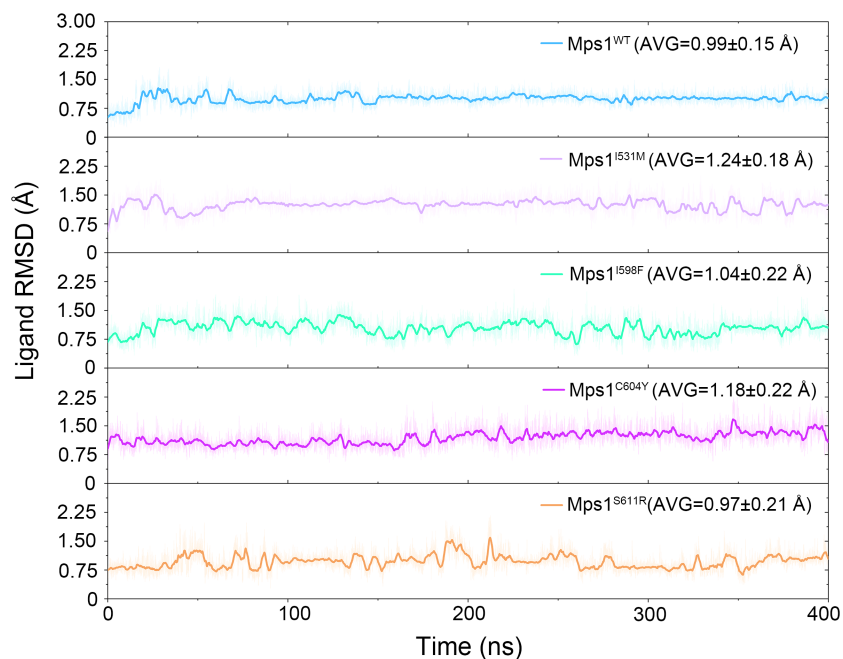
Full-size 🖼 DOI: 10.7717/peerj.6299/fig-7

Figure 8 **Time evolution of the RMSD values of Cpd-5 in the five studied systems from GaMD simulations.** The values reflect the equilibration of Cpd-5 in different protein relative to the initial structures.

Full-size 🖼 DOI: 10.7717/peerj.6299/fig-8
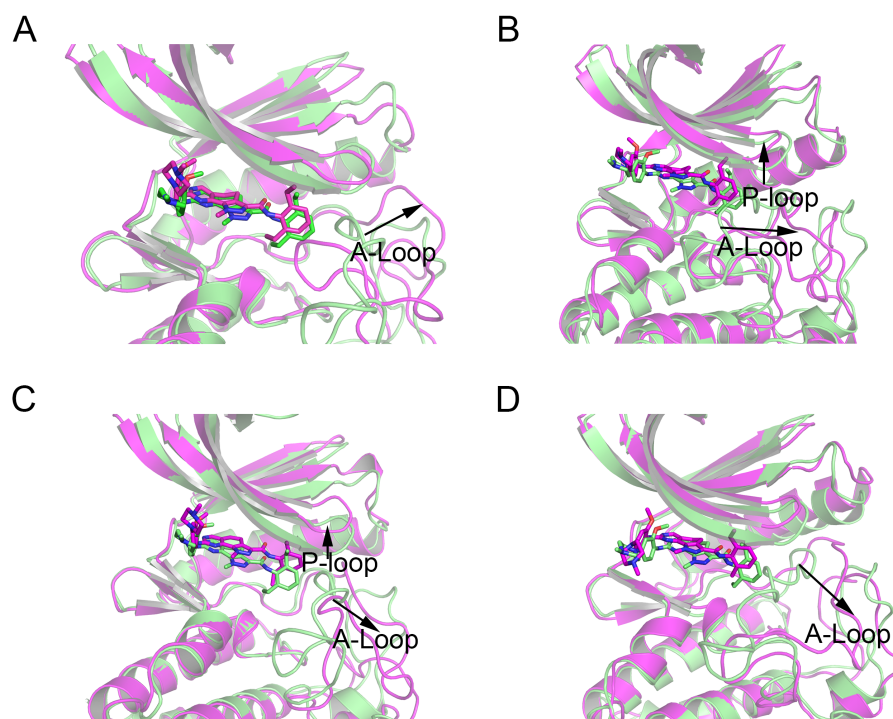
Figure 9 **Alignment of the last snapshot between Mps1^{WT}/cpd-5 and the mutant systems from GaMD simulations.** (A) Mps1^{WT}/cpd-5 (lime) and Mps1^{I531M}/Cpd-5 (magenta). (B) Mps1^{WT}/cpd-5 (lime) and Mps1^{I598F}/Cpd-5 (magenta). (C) Mps1^{WT}/cpd-5 (lime) and Mps1^{C604Y}/Cpd-5 (magenta). (D) Mps1^{WT}/cpd-5 (lime) and Mps1^{S611R}/Cpd-5 (magenta).

Full-size 🖼 DOI: 10.7717/peerj.6299/fig-9

In addition, the average RMSD values of both the protein and the ligand follow the order of WT systems <mutant systems, which are similar with the results from the conventional MD simulation. The above observations suggested that these four point mutations allowed larger conformational changes and more variability among protein subunits. Then, the last snapshots of each mutant system (magenta) extracted from GaMD simulation trajectories were superimposed with the last snapshot of WT system (green) to obtain an intuitionistic description of the conformational changes among these systems. As shown in Figs. 9A–9D, most conformational changes occurred in the P-loop and A-loop. These findings also supported the observation from conventional MD simulations. Compared with Mps1^{WT}, the P-loop of Mps1^{I598F}, Mps1^{C604Y}, and A-loop of all the mutant systems changed into upward-moving conformations and outward-moving conformations, respectively.

PCA was performed to further characterize the conformational transitions and plotted against time (Fig. 10). PCA reduces the dimensionality of large data sets and the vectors with the highest eigenvalues represent the most significant principal components (PCs). When principal components are plotted against each other, similar structures are clustered. Theoretically, each cluster shows a different protein conformational state. As shown in Fig. 10 and Fig. S1, the conformational states of both the WT and mutant systems were dynamics and functions during 0–400 ns GaMD simulations, and finally, stabilized in one state. Compared to the WT system, the mutant systems exhibited more structural clusters
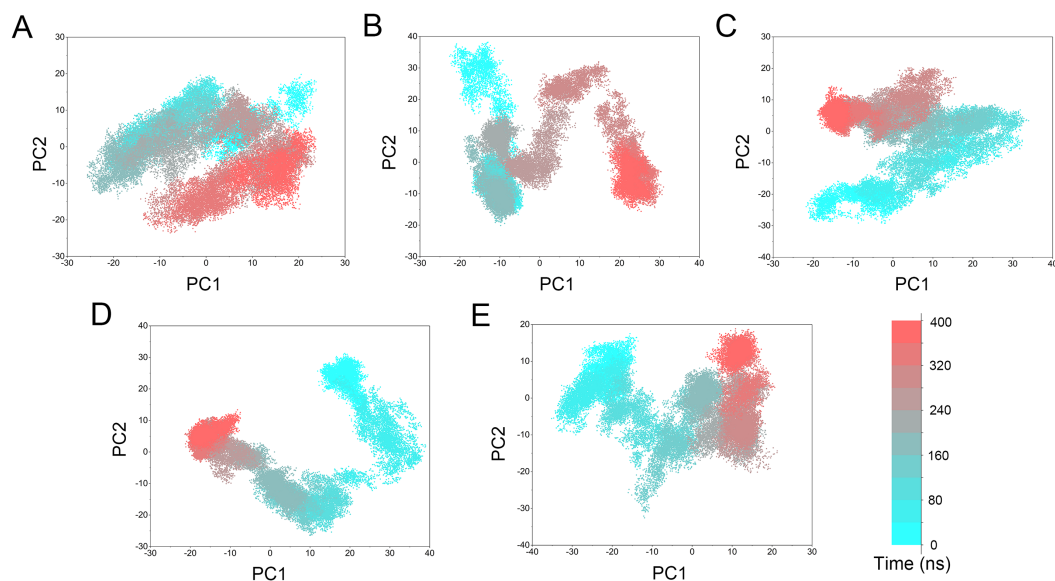
Figure 10 **PCA scatter plot of 50,000 snapshots from GaMD simulations along the first two principal components and plotted against time.** (A) Mps1^{WT}/cpd-5. (B) Mps1^{I531M}/Cpd-5 (magenta). (C) Mps1^{I598F}/Cpd-5. (D) Mps1^{C604Y}/Cpd-5; (E) Mps1^{S611R}/Cpd-5.

Full-size ⬛ DOI: 10.7717/peerj.6299/fig-10

and larger eigenvalues. These conformer plots highlighted the major differences between WT and mutant systems, which interpreted the observations of large conformational changes when resistance mutations occurred by conventional MD simulations and GaMD simulations.

The free energy landscape was utilized to further explain the relationship between the conformational change and energetic change. More energetic wells (dark blue regions) represent the protein underwent larger conformational change. As shown in Fig. 11, the WT system was confined to a major energetic deep well throughout the simulation (Fig. 11A), while numerous of energetic deep wells were observed for the four mutant systems (Figs. 11B–11F), highlighting an ensemble of different conformational states distributed over a large free energy space. Additionally, the free energy landscape between the four mutant systems also showed significant difference (Figs. 11B–11F), suggesting the four mutations may allosterically regulate the conformational ensemble to induce inhibitors resistance.

CONCLUSIONS

In this study, molecular modeling, conventional MD simulations and GaMD simulations successfully clarified the resistance mechanism induced by the four point mutations of I531M, I598F, C604Y, S611R, both structurally and energetically. The binding free energies of Cpd-5 to the WT system and mutant systems were well predicted and the decomposition of the individual energy terms suggested the major variation of Cpd-5 between the WT system and the mutant systems were van der Waals interactions. Structural analysis revealed the conformational changes of the P-loop, A-loop and αC-helix play crucial role for Cpd-5
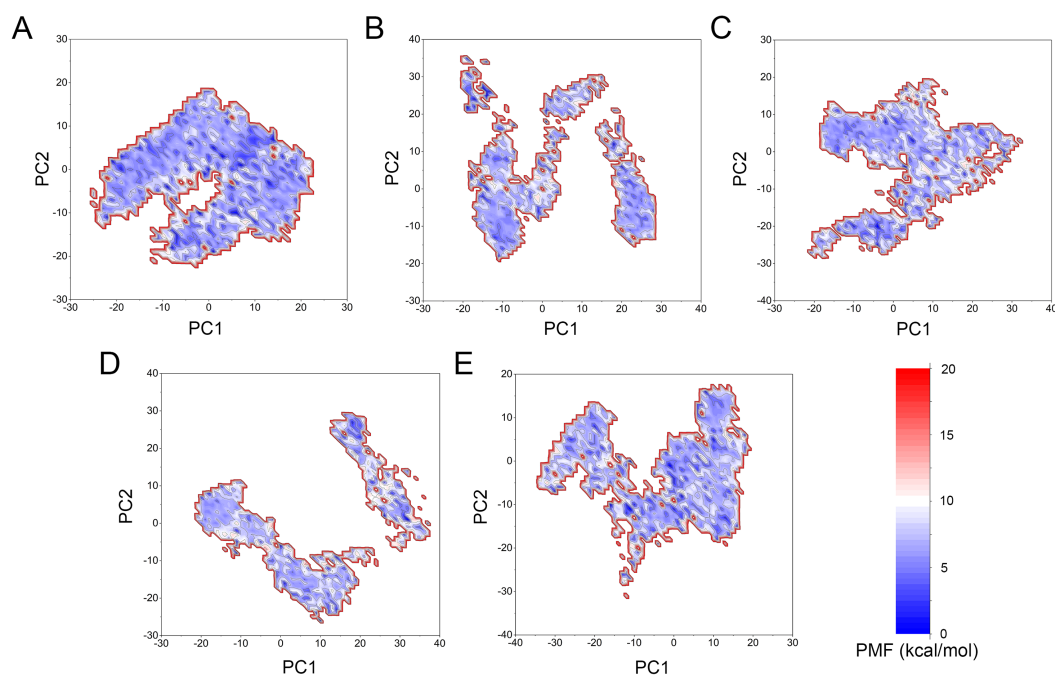
Figure 11 Two-dimensional free energy landscape of the first and second principal components calculated from GaMD simulations. (A) Mps1^{WT}/cpd-5. (B) Mps1^{I531M}/Cpd-5 (magenta). (C) Mps1^{I598F}/Cpd-5. (D) Mps1^{C604Y}/Cpd-5. (E) Mps1^{S611R}/Cpd-5.

Full-size 🖼 DOI: 10.7717/peerj.6299/fig-11

resistance. Further energetic differences of per-residue between the WT system and the mutant systems revealed the four mutations may allosterically regulate the conformational ensemble and the major variations were residues of Ile-663 and Gln-683, which were located in the key loops of catalytic loop and A-loop, respectively. In addition, GaMD simulations supported the observations from conventional MD simulations. PCA results and free energy landscape from GaMD simulations indicated Mps1 underwent large conformational changes when the resistance mutations occurred. In summary, our study not only revealed the resistance determinants of Cpd-5 to the four point mutations, but also provides some valuable information for structure based design of novel inhibitors of Mps1 in the future.

ADDITIONAL INFORMATION AND DECLARATIONS

Competing Interests

The authors declare there are no competing interests.

Author Contributions

- Yan Han conceived and designed the experiments, performed the experiments, approved the final draft.
- Yungang Wu conceived and designed the experiments, performed the experiments, analyzed the data, contributed reagents/materials/analysis tools, prepared figures and/or tables, authored or reviewed drafts of the paper, approved the final draft.
- Yi Xu conceived and designed the experiments, performed the experiments, analyzed the data, contributed reagents/materials/analysis tools, prepared figures and/or tables.
- Wentao Guo performed the experiments, analyzed the data, contributed reagents/materials/analysis tools.
- Na Zhang performed the experiments, authored or reviewed drafts of the paper.
- Xiaoyi Wang conceived and designed the experiments, authored or reviewed drafts of the paper.

Data Availability

The following information was supplied regarding data availability:
Raw data is available in the Supplemental Files.

Supplemental Information

Supplemental information for this article can be found online at http://dx.doi.org/10.7717/peerj.6299#supplemental-information.

REFERENCES

Barnum KJ, O'Connell MJ. 2014. Cell cycle regulation by checkpoints. *Methods in Molecular Biology* **1170**:29–40 DOI 10.1007/978-1-4939-0888-2_2.

Bertoli C, Skotheim JM, De Bruin RA. 2013. Control of cell cycle transcription during G1 and S phases. *Nature Reviews Molecular Cell Biology* **14**:518–528 DOI 10.1038/nrm3629.

Chen Y, Yu W, Jiang CC, Zheng JG. 2018. Insights into resistance mechanisms of inhibitors to Mps1 C604Y mutation via a comprehensive molecular modeling study. *Molecules* **23**(**6**):1488 DOI 10.3390/molecules23061488.

Chu ML, Chavas LM, Douglas KT, Eyers PA, Tabernero L. 2008. Crystal structure of the catalytic domain of the mitotic checkpoint kinase Mps1 in complex with SP600125. *Journal of Biological Chemistry* **283**:21495–21500 DOI 10.1074/jbc.M803026200.

Colombo R, Caldarelli M, Mennecozzi M, Giorgini ML, Sola F, Cappella P, Perrera C, Depaolini SR, Rusconi L, Cucchi U, Avanzi N, Bertrand JA, Bossi RT, Pesenti E, Galvani A, Isacchi A, Colotta F, Donati D, Moll J. 2010. Targeting the mitotic checkpoint for cancer therapy with NMS-P715, an inhibitor of MPS1 kinase. *Cancer Research* **70**:10255–10264 DOI 10.1158/0008-5472.CAN-10-2101.

Daniel J, Coulter J, Woo JH, Wilsbach K, Gabrielson E. 2011. High levels of the Mps1 checkpoint protein are protective of aneuploidy in breast cancer cells. *Proceedings of the National Academy of Sciences of the United States of America* **108**:5384–5389 DOI 10.1073/pnas.1007645108.

De Carcer G, Perez de Castro I, Malumbres M. 2007. Targeting cell cycle kinases for cancer therapy. *Current Medicinal Chemistry* **14**:969–985 DOI 10.2174/092986707780362925.

Essmann U, Perera L, Berkowitz ML, Darden T, Lee H, Pedersen LG. 1995. A smooth particle mesh Ewald method. *The Journal of Chemical Physics* **103**:8577–8593 DOI 10.1063/1.470117.

Fiser A, Sali A. 2003. Modeller: generation and refinement of homology-based protein structure models. *Methods in Enzymology* **374**:461–491 DOI 10.1016/S0076-6879(03)74020-8.

He M, Li W, Zheng Q, Zhang H. 2018. A molecular dynamics investigation into the mechanisms of alectinib resistance of three ALK mutants. *Journal of Cellular Biochemistry* **119**:5332–5342 DOI 10.1002/jcb.26666.

Hewitt L, Tighe A, Santaguida S, White AM, Jones CD, Musacchio A, Green S, Taylor SS. 2010. Sustained Mps1 activity is required in mitosis to recruit O-Mad2 to the Mad1-C-Mad2 core complex. *Journal of Cell Biology* **190**:25–34 DOI 10.1083/jcb.201002133.

Hiruma Y, Koch A, Hazraty N, Tsakou F, Medema RH, Joosten RP, Perrakis A. 2017. Understanding inhibitor resistance in Mps1 kinase through novel biophysical assays and structures. *Journal of Biological Chemistry* **292**:14496–14504 DOI 10.1074/jbc.M117.783555.

Hiruma Y, Sacristan C, Pachis ST, Adamopoulos A, Kuijt T, Ubbink M, Von Castelmur E, Perrakis A, Kops GJ. 2015. CELL DIVISION CYCLE. Competition between MPS1 and microtubules at kinetochores regulates spindle checkpoint signaling. *Science* **348**:1264–1267 DOI 10.1126/science.aaa4055.

Izaguirre JA, Catarello DP, Wozniak JM, Skeel RD. 2001. Langevin stabilization of molecular dynamics. *The Journal of Chemical Physics* **114**:2090–2098 DOI 10.1063/1.1332996.

Koch A, Maia A, Janssen A, Medema RH. 2016. Molecular basis underlying resistance to Mps1/TTK inhibitors. *Oncogene* **35**:2518–2528 DOI 10.1038/onc.2015.319.

Kräutler V, Van Gunsteren WF, Hünenberger PH. 2001. A fast SHAKE algorithm to solve distance constraint equations for small molecules in molecular dynamics simulations. *Journal of Computational Chemistry* **22**:501–508 DOI 10.1002/1096-987X(20010415)22:5<501::AID-JCC1021>3.0.CO;2-V.

Kuntal BK, Aparoy P, Reddanna P. 2010. EasyModeller: a graphical interface to MODELLER. *BMC Research Notes* **3**:226 DOI 10.1186/1756-0500-3-226.

Liu HL, Zhong HY, Song TQ, Li JZ. 2017. A molecular modeling study of the hydroxyflutamide resistance mechanism induced by androgen receptor mutations. *International Journal of Molecular Sciences* **18(9)**:1823 DOI 10.3390/ijms18091823.

Marques S, Fonseca J, Silva PM, Bousbaa H. 2015. Targeting the spindle assembly checkpoint for breast cancer treatment. *Current Cancer Drug Targets* **15**:272–281 DOI 10.2174/1568009615666150302130010.

Miao Y, McCammon JA. 2016a. Graded activation and free energy landscapes of a muscarinic G-protein-coupled receptor. *Proceedings of the National Academy of Sciences of the United States of America* **113**:12162–12167 DOI 10.1073/pnas.1614538113.

Miao Y, McCammon JA. 2016b. Unconstrained enhanced sampling for free energy calculations of biomolecules: a review. *Molecular Simulation* **42**:1046–1055 DOI 10.1080/08927022.2015.1121541.

Miao Y, Sinko W, Pierce L, Bucher D, Walker RC, McCammon JA. 2014. Improved reweighting of accelerated molecular dynamics simulations for free energy calculation. *Journal of Chemical Theory and Computation* **10**:2677–2689 DOI 10.1021/ct500090q.

Naud S, Westwood IM, Faisal A, Sheldrake P, Bavetsias V, Atrash B, Cheung KM, Liu M, Hayes A, Schmitt J, Wood A, Choi V, Boxall K, Mak G, Gurden M, Valenti M, De Haven Brandon A, Henley A, Baker R, McAndrew C, Matijssen B, Burke R, Hoelder S, Eccles SA, Raynaud FI, Linardopoulos S, Van Montfort RL, Blagg J. 2013. Structure-based design of orally bioavailable 1H-pyrrolo[3, 2-c] pyridine inhibitors of mitotic kinase monopolar spindle 1 (MPS1). *Journal of Medicinal Chemistry* **56**:10045–10065 DOI 10.1021/jm401395s.

Onufriev A, Bashford D, David A. 2000. Modification of the generalized Born model suitable for macromolecules. *The Journal of Physical Chemistry* **104**:3712–3720.

Pachis ST, Kops G. 2018. Leader of the SAC: molecular mechanisms of Mps1/TTK regulation in mitosis. *Open Biology* **8**:180109 DOI 10.1098/rsob.180109.

Pan P, Li Y, Yu H, Sun H, Hou T. 2013. Molecular principle of topotecan resistance by topoisomerase I mutations through molecular modeling approaches. *Journal of Chemical Information and Modeling* **53**:997–1006 DOI 10.1021/ci400066x.

Pettersen EF, Goddard TD, Huang CC, Couch GS, Greenblatt DM, Meng EC, Ferrin TE. 2004. UCSF Chimera—a visualization system for exploratory research and analysis. *Journal of Computational Chemistry* **25**:1605–1612 DOI 10.1002/jcc.20084.

Roe DR, Cheatham 3rd TE. 2013. PTRAJ and CPPTRAJ: software for processing and analysis of molecular dynamics trajectory data. *Journal of Chemical Theory and Computation* **9**:3084–3095 DOI 10.1021/ct400341p.

Salmela AL, Kallio MJ. 2013. Mitosis as an anti-cancer drug target. *Chromosoma* **122**:431–449 DOI 10.1007/s00412-013-0419-8.

Skjaerven L, Yao XQ, Scarabelli G, Grant BJ. 2014. Integrating protein structural dynamics and evolutionary analysis with Bio3D. *BMC Bioinformatics* **15**:399 DOI 10.1186/s12859-014-0399-6.

Sun H, Li Y, Li D, Hou T. 2013. Insight into crizotinib resistance mechanisms caused by three mutations in ALK tyrosine kinase using free energy calculation approaches. *Journal of Chemical Information and Modeling* **53**:2376–2389 DOI 10.1021/ci400188q.

Tannous BA, Kerami M, Van der Stoop PM, Kwiatkowski N, Wang J, Zhou W, Kessler AF, Lewandrowski G, Hiddingh L, Sol N, Lagerweij T, Wedekind L, Niers JM, Barazas M, Nilsson RJ, Geerts D, De Witt Hamer PC, Hagemann C, Vandertop WP, Van Tellingen O, Noske DP, Gray NS, Wurdinger T. 2013. Effects of the selective MPS1 inhibitor MPS1-IN-3 on glioblastoma sensitivity to antimitotic drugs. *Journal of the National Cancer Institute* **105**:1322–1331 DOI 10.1093/jnci/djt168.

Tardif KD, Rogers A, Cassiano J, Roth BL, Cimbora DM, McKinnon R, Peterson A, Douce TB, Robinson R, Dorweiler I, Davis T, Hess MA, Ostanin K, Papac DI, Baichwal V, McAlexander I, Willardsen JA, Saunders M, Christophe H, Kumar DV, Wettstein DA, Carlson RO, Williams BL. 2011. Characterization of the cellular and antitumor effects of MPI-0479605, a small-molecule inhibitor of the mitotic kinase Mps1. *Molecular Cancer Therapeutics* **10**:2267–2275 DOI 10.1158/1535-7163.MCT-11-0453.

Wang W, Yang Y, Gao Y, Xu Q, Wang F, Zhu S, Old W, Resing K, Ahn N, Lei M, Liu X. 2009. Structural and mechanistic insights into Mps1 kinase activation. *Journal of Cellular and Molecular Medicine* **13**:1679–1694 DOI 10.1111/j.1582-4934.2008.00605.x.

Xie Y, Wang A, Lin J, Wu L, Zhang H, Yang X, Wan X, Miao R, Sang X, Zhao H. 2017. Mps1/TTK: a novel target and biomarker for cancer. *Journal of Drug Targeting* **25**:112–118 DOI 10.1080/1061186X.2016.1258568.